Earth and Planetary Science Letters 435 (2016) 1–13

Contents lists available at ScienceDirect

Earth and Planetary Science Letters

www.elsevier.com/locate/epsl

Development of a novel empirical framework for interpreting geological carbon isotope excursions, with implications for the rate of carbon injection across the PETM

Sandra Kirtland Turner [a,b,*], Andy Ridgwell [b,a]

[a] Department of Earth Sciences, University of California, Riverside, Riverside, CA 92521, USA
[b] School of Geographical Sciences, University of Bristol, Bristol BS8 1SS, UK

ARTICLE INFO

Article history:
Received 27 March 2015
Received in revised form 11 November 2015
Accepted 19 November 2015
Available online 14 December 2015
Editor: H. Stoll

Keywords:
PETM
carbon isotopes
Earth system modeling

ABSTRACT

As an episode of rapid global warming associated with the release of massive quantities of carbon to the atmosphere and oceans, the Paleocene–Eocene Thermal Maximum (PETM, ~56 Ma) is considered a potential analog for modern anthropogenic carbon emissions. However, the prevailing order of magnitude uncertainty in the rate of carbon release during the PETM precludes any straightforward comparison between the paleo-record and the modern. Similar barriers exist to the interpretation of many other carbon isotope excursions in the geological record. Here we use the Earth system model cGENIE to quantify the consequences of differing carbon emissions rates on the isotopic record of different carbon reservoirs. We explore the consequences of a range of emissions scenarios – from durations of carbon input of years to millennia and constant versus pulsed emissions rates, and trace how the isotopic signal is imprinted on the different carbon reservoirs. From this, we identify a characteristic relationship between the difference in carbon isotope excursion sizes between atmospheric CO_2 and dissolved inorganic carbon (DIC) and the duration of carbon emissions. To the extent that available isotopic data spanning the PETM constrain the size of the marine and atmospheric carbon isotopic excursions, applying this empirical relationship suggests the duration of the component of carbon emissions that dominates the isotopic signal could be less than 3000 yr. However, utilizing the ratio of excursion size in the atmosphere to ocean as a metric to constrain duration of carbon emissions highlights the necessity to strengthen estimates for these two measurements across the PETM. Our general interpretive framework could be equally applied in assessing rates of carbon emissions for other geological events.

1. Introduction

The Paleocene–Eocene Thermal Maximum (PETM, ~56 Ma) is the most well-studied example of a hyperthermal event and perhaps our best geologic analog for future climate change. Hyperthermals like the PETM are identified in the sedimentary record by three primary lines of evidence: 1) a negative carbon isotopic ($\delta^{13}C$) excursion (CIE) (McInerney and Wing, 2011; Zachos et al., 2008), 2) dissolution of marine carbonates ($CaCO_3$) (Zachos et al., 2005), and 3) a transient increase in temperature indicated by paleotemperature proxies (Dunkley Jones et al., 2013; Zachos et al., 2008). Together, these lines of evidence are consistent with the PETM being driven by massive release of isotopically depleted carbon to the atmosphere and oceans, leading to warming and ocean acidification (Hönisch et al., 2012). However, a comparison between the rate of onset and current anthropogenic emissions of ~10 Pg C yr^{-1} (Peters et al., 2012) is fundamental to drawing any future analogy (Hönisch et al., 2012).

Even for an event as well-studied as the PETM, there is currently no widely agreed upon common age model to constrain the onset phase any more precisely than 5–20 kyr (McInerney and Wing, 2011). The invariably slow accumulation time of deep sea sediments, combined with the influence of bioturbation and reduced deposition or chemical erosion of carbonates (Ridgwell, 2007) presents a challenge for constraining the event onset (Zachos et al., 2005). Yet, these records tend to have by far the most complete age model constraints through biostratigraphic and magnetostratigraphic markers, astronomical cycle counts, and measurements of constant sedimentation rate proxies, such as the flux of extraterrestrial ^3He (Farley and Eltgroth, 2003; Rohl et al., 2007). Age models derived from deep sea sites are hence often applied to

* Corresponding author at: Department of Earth Sciences, University of California, Riverside, Riverside, CA 92521, USA.
E-mail address: sandra.kirtlandturner@ucr.edu (S. Kirtland Turner).

http://dx.doi.org/10.1016/j.epsl.2015.11.027

records from shallow marine and terrestrial settings on the basis of carbon isotope stratigraphy (e.g. Bowen and Beitler Bowen, 2008; Cui et al., 2011) but this makes hitherto unquantified assumptions about the relative shape of the excursion among various settings. Orbital tuning of such sections relies on accurate identification of short astronomical cycles (precession) and assumes linear sedimentation between tie points, sufficient only to say that the onset of the PETM apparently occurred within a single precession cycle (19 kyr) (Cui et al., 2011). No reliable direct age control at millennial or shorter timescales exists.

There is also uncertainty regarding the magnitude of the carbon isotopic excursion (McInerney and Wing, 2011). This is important because the CIE size, combined with the magnitude of change in ocean saturation state, should theoretically constrain the mass and isotopic composition of the carbon source (Panchuk et al., 2008; Zeebe et al., 2009). Similar to uncertainty over age models for the PETM onset, site-to-site variations in the size of the CIE and a lack of constraints on the evolution of ocean carbonate chemistry across the event mean that the best estimates for the mass of carbon released across the PETM still span a factor of two or more – from perhaps 3000 to 6000 Pg C with an isotopic composition somewhere between methane ($\sim -60‰$) and organic carbon (-22 to $-27‰$) (Panchuk et al., 2008; Zeebe et al., 2009).

Deep sea benthic foraminiferal records sample the dissolved inorganic carbon (DIC) reservoir, which dominates the mass of the exogenic carbon pool and should thus provide the closest estimate for the global CIE size, yet benthic foraminiferal CIEs are also observed to vary in magnitude from site to site (Sluijs and Dickens, 2012). Further, the resolution of these records is limited by the mixing time of the oceans, as well as the rate of sediment accumulation and the depth of mixing in the sediments, such that even a record which perfectly sampled the CIE in the oceanic DIC pool would not constrain the duration of carbon release if it was faster than the ocean's mixing time – an effect potentially complicated by changes in ocean mixing time in response to warming (i.e. transient stratification) (Thomas et al., 2002). Records of the CIE from marine organic carbon avoid the potential for truncation by chemical erosion, but these records are potentially biased by changes in the composition of organic matter (terrestrial vs. marine) as well as changes in fractionation during organic carbon fixation because of elevated atmospheric pCO_2 – factors which can either dampen or amplify the recorded CIE (Cui et al., 2011; Sluijs and Dickens, 2012). Similarly, $\delta^{13}C$ records from soil carbonates are not subject to dissolution or bioturbation, but the CIE magnitude may be biased by changes in vegetation, hydrology, and soil formation (Bowen and Beitler Bowen, 2008; Dunkley Jones et al., 2010). Overall, marine and terrestrial CIEs are significantly different, with terrestrial records consistently indicating a larger perturbation (McInerney and Wing, 2011).

Given the diversity of carbon reservoirs and variability in the size of recorded CIEs, a means of quantifying the expected CIE size relationship is needed to support the interpretation of an event. Here we use the Earth system model cGENIE (Edwards and Marsh, 2005; Ridgwell and Hargreaves, 2007; Ridgwell et al., 2007) to provide a general theoretical framework for interpreting abrupt onset ($<$20 kyr) CIEs in the geologic record and to quantify how such anomalies propagate through various reservoirs within the exogenic carbon pool, excluding biases entrained during the formation of the sedimentary record. We take the PETM as a case study as it continues to be identified from a wide range of depositional settings and substrates and employ a late Paleocene configuration of the model. We go on to demonstrate how varying rates of carbon release will generate predictable differences in the size and time-history of the CIE preserved from various reservoirs, an approach that may help bypass the difficulty of generating accurate age models for rapid events and explain apparent inter-site discrepancies in the size of global CIEs.

2. Methods

In this paper we employ 'cGENIE' – an Earth system model of intermediate complexity comprising: a 3-D dynamic ocean circulation model with simplified 'energy and moisture' balance atmosphere (Edwards and Marsh, 2005), a representation of the biogeochemical cycling of elements and isotopes in the ocean (Ridgwell et al., 2007), plus marine sediments (Ridgwell and Hargreaves, 2007) and terrestrial weathering (Colbourn et al., 2013) to close the geological cycle of carbon. Because of the inherent importance of achieving an appropriate simile of carbon isotope dynamics in the ocean and atmosphere, we provide an overview and assessment of the cGENIE ^{13}C cycle, before describing the experimental methodology.

2.1. Representation and evaluation of $\delta^{13}C$ in cGENIE

The ^{13}C cycle in cGENIE is based on the scheme described in Ridgwell (2001) and updated as described in Ridgwell et al. (2007). In brief: solution of the isotopic partitioning of carbon between the different aqueous carbonate species (i.e., $CO_{2(aq)}$, HCO_3^-, CO_3^{2-}) follows Zeebe and Wolf-Gladrow (2001) (their Section 3.2) in which the fractionation factors are from Zhang et al. (1995). The air–sea fractionation scheme follows that of Marchal et al. (1998) with the individual fractionation factors all taken from Zhang et al. (1995). Air–sea fractionation is a function of both kinetic and equilibrium fractionation effects (the latter of which is dependent on temperature) while sea–air fractionation is a function of kinetic fractionation and also takes into account carbonate speciation in seawater. For the formation of organic matter at the ocean surface, fractionation occurs with respect to $\delta^{13}C$ of $CO_{2(aq)}$, and is a function of the $CO_{2(aq)}$ concentration in an approximation (Ridgwell, 2001) of the model of Rau et al. (1996). Fractionation between the $\delta^{13}C$ of HCO_3^- and calcite follows Mook (1986) in a simple temperature-only dependency. The cGENIE model hence incorporates all the major ocean–atmosphere, biotic and abiotic ^{13}C fractionations, together with the relevant dependencies on temperature, $[CO_{2(aq)}]$, and pH. The notable exceptions are: exchange with the terrestrial biosphere and any foraminiferal ^{13}C vital effect dependency on ambient carbonate ion concentration.

As a result of the ongoing release of isotopically depleted fossil fuel-derived CO_2 to the atmosphere, there exist no measurements of the pre-industrial steady-state distribution of the $\delta^{13}C$ of dissolved inorganic carbon ($\delta^{13}C_{(DIC)}$). This requires a more realistic test of cGENIE when made against modern observations, because the model needs to not only reasonably simulate the large-scale and deep-ocean steady state distributions of $\delta^{13}C_{(DIC)}$, but also the decadal-scale dynamic propagation of the fossil fuel CO_2 signal from the surface to intermediate depths. Available compilations of $\delta^{13}C_{(DIC)}$ observations (Schmittner et al., 2013) span 1990 to 2005. To create a comparable model field, we take a modern configuration of cGENIE (Cao et al., 2009) with the same resolution as used subsequently for the Eocene (see Section 2.2) and run it through a standardized forced historical atmospheric transient (see: Cao et al., 2009, until year 2010). We extract the annual average for the year 1998 from the model as approximately representative of the data.

We illustrate the model-data evaluation in a single plot (Fig. 1) comprising model-generated fields of $\delta^{13}C_{(DIC)}$ that have been zonally-averaged across each present-day ocean basin, together with anomaly fields of model minus the observations of Schmittner et al. (2013) re-gridded to the same model grid. (Statistical summary plots are given in the SI as Fig. S1a–d.) The model reason-

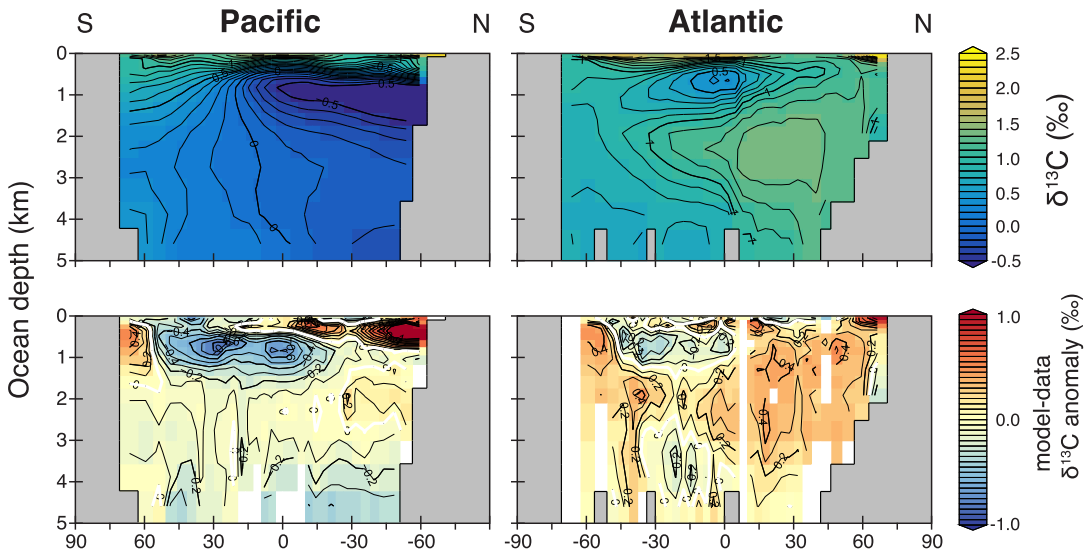

Fig. 1. Evaluation of the global $\delta^{13}C$ cycle in cGENIE. Shown in the top two panels for present-day Atlantic (right) and Pacific (left) basins, is the zonally-averaged $\delta^{13}C$ profile of DIC corresponding to year 1998. In the lower two panels are the corresponding zonal anomalies of model year 1998 minus observed $\delta^{13}C$ DIC data (years 1990–2005) (Schmittner et al., 2013).

ably captures the deep and surface ocean $\delta^{13}C_{(DIC)}$ observational values, especially in the Pacific ($R^2 = 0.66$, $n = 2642$). In the Atlantic ($R^2 = 0.40$, $n = 846$), there is an over-prediction in $\delta^{13}C_{(DIC)}$ (ca. 0.3‰) throughout much of the Northern Hemisphere interior ocean, either due to imperfections in the volume and ventilation age of the North Atlantic deep water and/or too-high surface water $\delta^{13}C_{(DIC)}$ at the locations of convection. Also apparent is an underestimate in $\delta^{13}C_{(DIC)}$ of Antarctic Intermediate Water – a feature also apparent in the Pacific section and likely a consequence of low model resolution. Finally, the water column in the North Pacific is too deeply mixed, leading to an insufficiently shallow $\delta^{13}C_{(DIC)}$ minimum. In summary: on a global mean basis (see SI), surface (reflecting suppression driven by rapid CO_2 release) and deep (reflecting steady-state global ocean ^{13}C cycling) are reproduced to within ±0.1‰ of 1990–2005 observations. Model-data deviations of up to ±0.3‰ occur at sub-surface (~200 m) and intermediate (~800 m) horizons, likely reflecting a combination of poorly-resolved intermediate water formation in the sub-Antarctic and potentially a bias in the prescribed depth profile of water column organic carbon remineralization.

2.2. Experimental methodology

For subsequent experiments, we applied the early Eocene configuration of Ridgwell and Schmidt (2010). In a 20 kyr initial spin-up of Eocene ocean circulation and carbon cycling, atmospheric CO_2 was set to 834 ppm with a $\delta^{13}C$ of −4.9‰ and weathering tracked sedimentary loss at all times (a 'closed' system, Ridgwell and Hargreaves, 2007). To bring the geological ^{13}C cycle into steady state, we ran the model for a further 500 kyr as an 'open' system including temperature-dependent silicate and carbonate weathering (Colbourn et al., 2013). The total weathering flux (14.7 Tmol Ca^{2+} yr^{-1}) needed to balance global carbonate burial was split 50:50 between carbonate and silicate weathering together with a volcanic outgassing flux of 7.35 Tmol C yr^{-1}. The $\delta^{13}C$ of volcanic outgassing was set to −6‰ and in the absence of organic carbon burial, the $\delta^{13}C$ of weathered carbonate was adjusted to balance the global $\delta^{13}C$ budget. To check for any potential impact of this isotopic mass balance approximation on our subsequent experiments, we also spun up the model as an open system incorporating a fixed 3.56 Tmol C yr^{-1} organic carbon burial flux in shallow sediments (<175 m water depth) at −26.2‰, rebalancing the input flux of volcanic CO_2 (increased to 10.9 Tmol C yr^{-1})

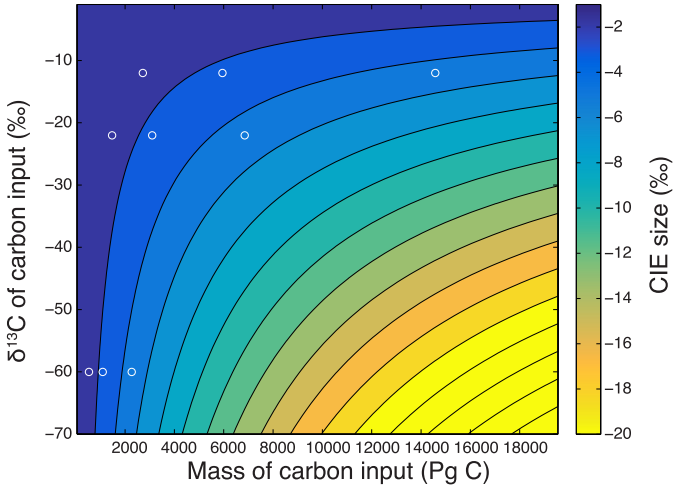

Fig. 2. Contour plot of CIE sizes (‰) as a function of the mass of carbon input (x-axis) and the $\delta^{13}C$ (‰) of the carbon input based on the total mass and $\delta^{13}C$ of the exogenic carbon reservoir in cGENIE. The exogenic reservoir in cGENIE includes atmospheric CO_2, oceanic DIC, and oceanic DOC and is equal to 32 356 Pg C with a $\delta^{13}C$ of 0.878‰. White circles indicate the combined mass and $\delta^{13}C$ of pulses applied to cGENIE to generate −1‰, −2‰, and −4‰ CIEs, respectively.

and setting the $\delta^{13}C$ of terrestrial carbonate weathering equal to marine carbonate burial (3.8‰). The two spin-up methodologies yielded no significant difference in steady state pCO_2 and $\delta^{13}C$ or in these values during transient experiments (see SI Fig. S2).

To trace the propagation of a carbon isotope anomaly through various carbon reservoirs in cGENIE we ran an ensemble of experiments, injecting carbon of a specified mass and $\delta^{13}C$ to the atmosphere to generate a range of CIEs. The required carbon input as a function of global CIE size and $\delta^{13}C$ of the carbon input was calculated as a simple steady-state mass balance (Fig. 2). Table S1 provides all the masses of applied carbon pulses in order to generate specified $\delta^{13}C$ excursions in cGENIE.

The selected $\delta^{13}C$ compositions for carbon pulses (−12‰, −22‰, and −60‰) span a range of proposed PETM sources (Panchuk et al., 2008; Zeebe et al., 2009), with the −12‰ source representing a mixture of mantle CO_2 and organic carbon and providing a high mass scenario (Panchuk et al., 2008). For each carbon release, we then varied the input duration from 1 to 10 000 yr (see

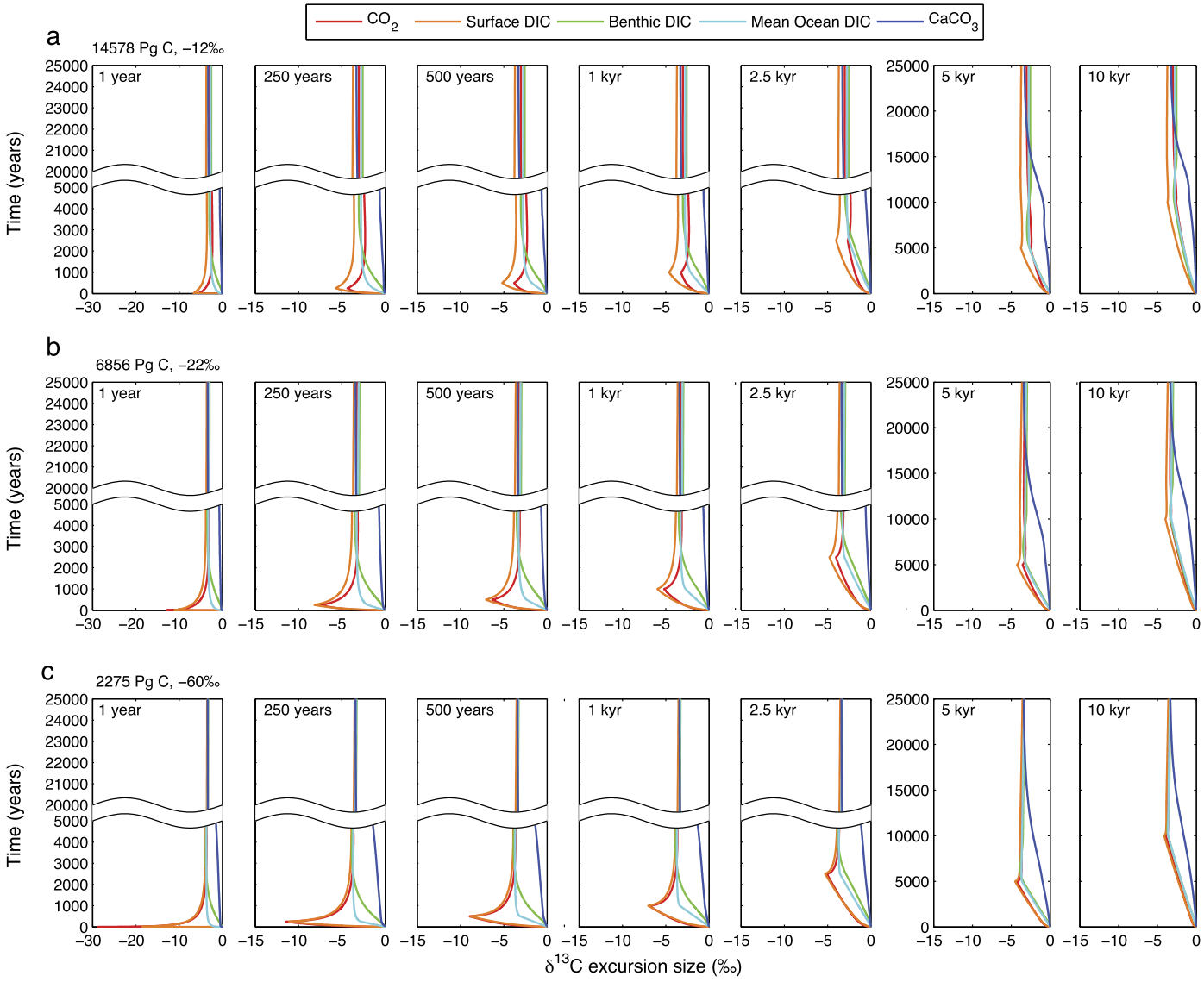

Fig. 3. Results of carbon release experiments with masses selected to generate a −4‰ global CIE and with varying durations of carbon input. a) carbon release of 14 578 Pg C of −12‰, b) carbon release of 6856 Pg C of −22‰ and c) carbon release of 2275 Pg C of −60‰. Results are shown for experiments (from left to right) with duration of carbon input 1, 250, 500, 1000, 2500, 5000, and 10 000 yr. Each line indicates the $\delta^{13}C$ with model time preserved in different modeled carbon reservoirs – atmospheric CO_2 in red, surface ocean dissolved inorganic carbon (DIC) in orange, benthic DIC in green, mean global ocean DIC in light blue, and sedimentary $CaCO_3$ in dark blue. Surface ocean DIC $\delta^{13}C$ is calculated as the average of all surface ocean grid cells (upper ~81 m of the modeled water column) and benthic DIC $\delta^{13}C$ is calculated as the average of all oceanic grid cells directly overlying sediments (variable water column depths). Mean ocean DIC $\delta^{13}C$ is calculated as the average of all oceanic grid cells. All $\delta^{13}C$ excursions are adjusted relative to 0‰ in order to trace the relative size of the excursion instead of the absolute $\delta^{13}C$ values recorded in each reservoir. For carbon release durations of ≤2500 yr, the *y*-axis has a break from 5000 to 20 000 yr, while there is no axis break for comparable plots with carbon release duration of 5000 and 10 000 yr.

Table S1), with carbon applied at a constant yearly rate equal to the total mass of carbon divided by the input duration. All experiments were run for 25 000 yr. For "PETM-equivalent" −4‰ CIE scenarios, we also ran all experiments without a CO_2-climate feedback and radiative forcing fixed at the equivalent of 834 ppm.

3. Results and discussion

3.1. Impact of onset duration on CIE size

For each Eocene carbon release experiment, the pulse of isotopically depleted carbon drives a negative CIE in atmosphere, ocean, and sedimentary carbon reservoirs. Fig. 3 shows the resulting $\delta^{13}C$ profiles for atmospheric CO_2, surface ocean DIC, mean ocean DIC, benthic DIC, and sedimentary $CaCO_3$ for each −4‰ CIE scenario with a varying input duration (1, 250, 500, 1000, 2500, 5000, and 10 000 yr experiments shown) (see Fig. S3a and b for equivalent −1‰ and −2‰ CIE time-series plots). For the mean ocean DIC, benthic DIC, and sedimentary $CaCO_3$ reservoirs, the input duration has little effect on the CIE magnitude (<0.2‰ difference when input duration varies from 1 to 10 000 yr; see Table S2), though the time-history of $\delta^{13}C$ differs, with slower excursion onsets for longer input durations. However, in the atmosphere and surface ocean DIC reservoirs, the CIE size is a strong function of the input duration (Fig. 3). Thus, the shorter the carbon input duration, the larger the amplification of the CIE in the atmosphere and surface ocean DIC pool relative to the deep ocean DIC pool. For very short input durations (<100 yr) and carbon pulses of −22 and −60‰, there is also an identifiable amplification of the CIE in the atmosphere relative to the surface ocean (see Table S2).

From the experiments, we identify a characteristic relationship for a given total emission between the duration of carbon input and the ratio of the size of the CIE in the atmosphere relative to the mean ocean DIC reservoir:

$$\frac{CIE_{ocn}}{CIE_{atm}} = a - b \cdot e^{-1 \cdot \frac{t_{onset}}{c}} \quad (1)$$

where CIE_{ocn} is the size of the CIE in the mean ocean DIC reservoir, CIE_{atm} is the size of the CIE in atmospheric CO_2, t_{onset} is the input duration in years, and a, b, and c are empirically determined constants that vary as a function of the mass of carbon input (Fig. 4). Table S3 provides constant values determined from −1‰, −2‰, and −4‰ CIE experiments with appropriate masses of carbon input given isotopic compositions of −12‰, −22‰, and −60‰. The complexity of multiple time-dependent fractionation processes coupled to advection of modeled carbon tracers necessitates the development of an empirical, rather than analytical, expression for the relationship describing the connection between the duration of atmospheric carbon injection and relative $\delta^{13}C$ excursion size.

3.2. Depth propagation of the $\delta^{13}C$ anomaly

Comparison of the modeled surface and mean ocean DIC $\delta^{13}C$ time series in Fig. 3 (and S3a and b) illustrates the time to propagate a $\delta^{13}C$ anomaly through the ocean. The difference in the timing of the $\delta^{13}C$ minimum in the surface ocean compared to the deep ocean shows an exponential decay relationship with input duration with the form:

$$t_{CIEbenthic} - t_{CIEsurf} = a \cdot e^{-b \cdot t_{onset}} \quad (2)$$

where t_{onset} is the input duration in years, $t_{CIEsurf}$ is the time of the $\delta^{13}C$ minimum in surface ocean DIC, $t_{CIEbenthic}$ is the time of the $\delta^{13}C$ minimum in benthic DIC, and a and b are empirically determined constants that vary as a function of the mass of carbon input (Fig. 5a, c, d). In experiments with radiative forcing fixed (Fig. 5b), the exponential decay relationship between the input duration and the delay in propagating the $\delta^{13}C$ anomaly from surface to deep is much weaker. Table S4 provides values for constants from all experiments with −22‰ or −60‰ inputs (and from −12‰ input when radiative forcing is fixed).

It is also possible to evaluate the time required to propagate ^{13}C-depleted carbon through each model ocean layer. cGENIE includes a 16 level ocean with maximum depth of 5 km and vertical spacing that increases with depth from ∼81 to ∼763 m. Fig. 6 shows the propagation of CIEs with ocean depth for 10 kyr following a carbon pulse of either −22‰ and −60‰ (with mass set in order to generate a −4‰ CIE) and varying input durations. Just as the 1-year release causes the largest delay in transmitting the $\delta^{13}C$ anomaly to the deep ocean (in Fig. 5), the delay is also greatest in moving the $\delta^{13}C$ minimum through each successive ocean layer (Fig. 6). The amplified CIEs (i.e. greater than the global CIE size of −4‰, marked by thick black contours in Fig. 6) created during the rapid release scenarios are restricted to the upper ∼1000 m of the modeled water column. As a result, during the onset phase of rapid release scenarios, absolute $\delta^{13}C$ values in the surface and deep-ocean will converge or even reverse, leading to a collapse in planktic–benthic $\Delta\delta^{13}C$ or negative planktic–benthic $\Delta\delta^{13}C$ within the first few thousand years following the onset of carbon release.

The relative amplification of the time it takes to propagate the CIE from the surface to the deep-ocean in experiments including CO_2-climate feedbacks is due to the relationship between global temperature and input duration. For a given CO_2 mass, faster release means a relatively larger increase in atmospheric pCO_2 and thus larger and faster increase in surface temperature (Fig. S4), driving transient ocean stratification. The longer-term (>5 kyr) response of circulation is to strengthen, with the magnitude of strengthening related to input duration, though less strongly than the initial weakening (Fig. S5). As a result, for rapid carbon release, the effect of CO_2-climate feedbacks is to increase the time it takes to propagate the $\delta^{13}C$ minimum to the deep-ocean, whereas for slower release (10 kyr input duration) CO_2-climate feedbacks actually decrease the time it takes to propagate the $\delta^{13}C$ minimum.

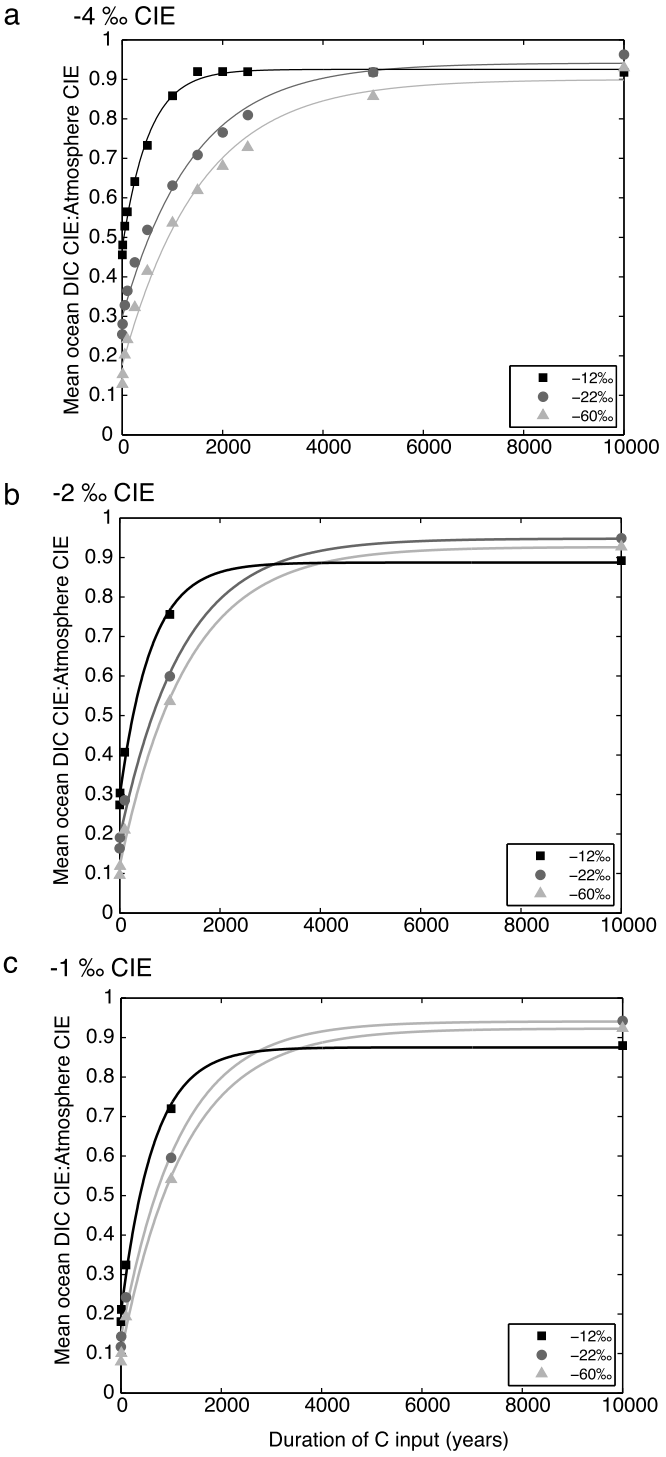

Fig. 4. Effect of duration of carbon release on the ratio of the CIE in mean global ocean DIC to atmospheric CO_2. Individual points are experiment results for −12‰ (black squares), −22‰ (dark grey circles) and −60‰ (light grey triangles) carbon pulses. Curve fits have the form of Eq. (1) – increasing form of exponential decay – with constants (and their error) provided in Table S3. a) −4‰ CIE experiment results, b) −2‰ CIE experiment results, and c) −1‰ CIE experiment results. Given a measured ratio between the mean ocean CIE and the atmosphere CIE, area between curves indicates the range of possible durations of carbon input.

Our empirical relationship between input duration and the delay in propagating the $\delta^{13}C$ minimum from the surface to deep ocean does not hold for −12‰ carbon input over longer durations because surface DIC $\delta^{13}C$ does not continuously recover to heavier

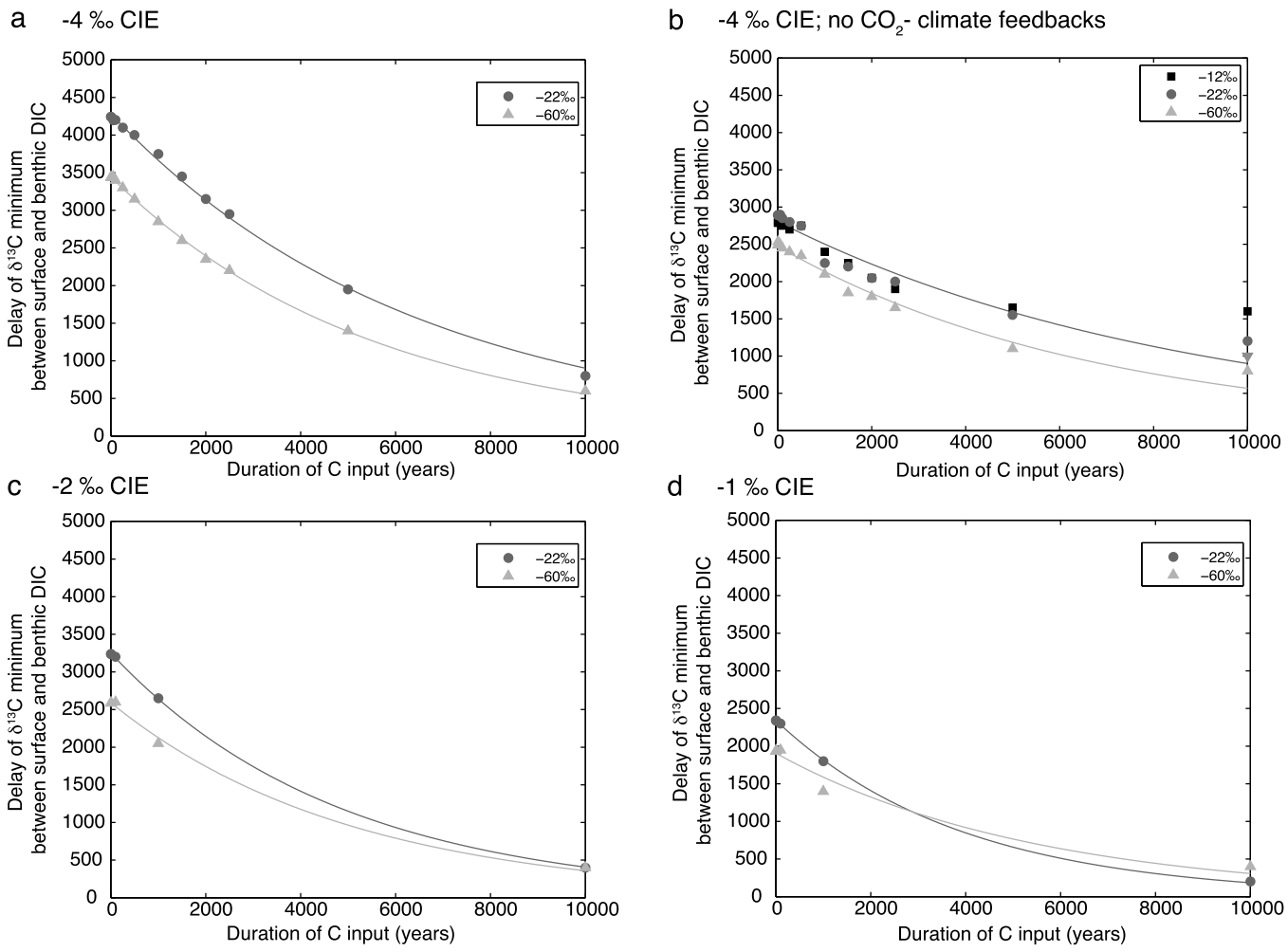

Fig. 5. Effect of duration of carbon release on the difference in the model time of the $\delta^{13}C$ minimum in surface ocean DIC compared to deep ocean DIC. Individual points are experiment results for −12‰ (black squares) and −22‰ (dark grey circles) carbon pulses. Curve fits have the form of Eq. (2) – exponential decay – with constants (and their error) provided in Table S4. a) −4‰ CIE experiment results, b) −4‰ CIE experiment results without CO_2-climate feedbacks, c) −2‰ CIE experiment results, and d) −1‰ CIE experiment results.

values after reaching the first $\delta^{13}C$ minimum. This is due to the extent of changes in ocean circulation caused by large masses of carbon release and does not occur in experiments where CO_2-climate feedbacks are fixed (Fig. 5b).

3.3. Impact of emissions rate on range in surface ocean CIEs

We also explore the range of CIE sizes that occur spatially within a single carbon reservoir. The degree to which a location at the ocean surface records a CIE originating in the atmosphere is some function of the local rate of air–sea gas exchange and upwelling/mixing as well as the local level of modeled productivity and its response to CO_2 release and warming. For longer carbon input durations where the size of the atmospheric CIE is diminished, surface ocean $\delta^{13}C$ tracks the atmospheric transient almost equally well everywhere and the range of CIE magnitudes recorded across the entire ocean surface is narrow (Fig. 7a). Conversely, for a fast release, the impact of differences in the air–sea gas exchange rate vs. mixing is amplified and the resulting range is large. For a given input duration, the CIE size range is also influenced by the total mass of carbon input, a phenomenon recognized by Panchuk (2007). Because the rate of air–sea gas exchange scales with the air–sea pCO_2 difference (Wanninkhof, 1992), the isotopic equilibrium is generally more complete and the CIE range smaller for larger total carbon releases (Fig. 7a). The situation becomes more complicated for slow releases approaching the time-scale of whole ocean mixing because of the influence of release mass on overturning, such that the larger mass leads to a larger CIE range for the same release rate.

Based on the above, releasing the isotopically lightest (−60‰) carbon in 1 yr will yield the largest range in surface ocean CIE sizes (Fig. 7a), hinting at a way of constraining input duration based on the variance in surface ocean records capturing a CIE. Another way to visualize the maximum range is by recording the time-history of surface DIC $\delta^{13}C$ in each wet grid cell (total of 905 locations) following a 1 year carbon pulse (Fig. 7b). While the mean surface DIC CIE is ∼20‰, the minimum is ∼10‰ and the maximum is ∼25‰. In this scenario, the atmospheric CIE is ∼30‰, so the smallest surface DIC CIE is approximately 1/3 the size of the atmospheric CIE. The minimum DIC CIEs also tend to occur more slowly – further indication that upwelling is suppressing the local record of the $\delta^{13}C$ perturbation.

3.4. How fast was the PETM onset?

Our experiments provide a theoretical framework for interpreting and constraining carbon input durations by comparing the magnitude of $\delta^{13}C$ change in records representing different reservoirs. Our empirical relationship between the ratio of the CIE in global oceanic DIC to atmospheric CO_2 and the carbon input du-

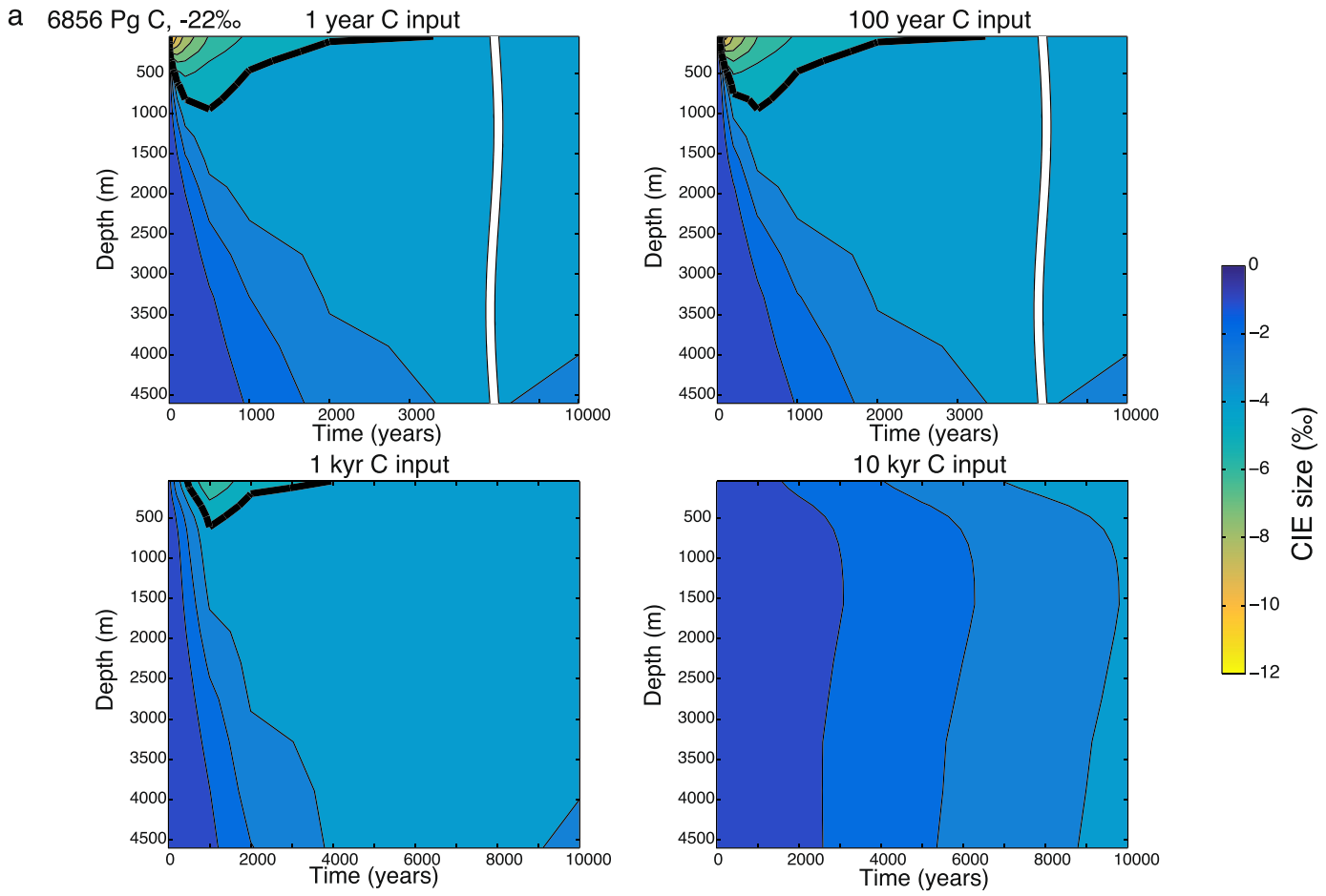

Fig. 6. Propagation of CIE with depth for the first 10 kyr following carbon release of varying durations. Plotted values are the average CIE in each model ocean layer. Thick black contour indicates a −4‰ CIE. Results are shown for a) −22‰ carbon input of 6856 Pg C and b) −60‰ carbon input of 2275 Pg C and durations of carbon input of 1 yr, 100 yr, 1000 yr, and 10 000 yr. For 1 yr and 100 yr releases, there is an *x*-axis break from 4000 to 9000 yr.

ration (Fig. 4, Table S3) is dependent on the total mass of carbon released, such that for a given CIE, the carbon input duration falls in a range constrained by the predicted mass of carbon input (Fig. 4). We use the PETM as a case study for applying our empirical relationship because of the large number of PETM $\delta^{13}C$ records generated from a wide variety of settings. Compilation of available PETM records suggests a statistically significant difference between mean marine (−2.8‰) and terrestrial reservoir (−4.7‰) CIE values (McInerney and Wing, 2011), which might be representative of the mean ocean and atmosphere, respectively. Using this assumption, the ratio of ∼0.6 would suggest a duration of onset between 167 and 1340 yr for isotopic pulses of −12‰ to −60‰, or 881–1340 yr for sources between −22‰ and −60‰.

However, the mean estimates of McInerney and Wing (2011) are arguably not representative of the whole ocean and atmosphere $\delta^{13}C$ excursions. For instance, biases among *n*-alkane records of different carbon chain length (Smith et al., 2007) or different plant groups (Schouten et al., 2007) may mean that terrestrial records do not perfectly record the atmospheric CO_2 excursion. Dissolution and mixing in deep-sea records can truncate the CIE and bias the mean marine CIE towards smaller values (Kirtland Turner and Ridgwell, 2013; Zachos et al., 2005).

In lieu of a mechanistic assessment of the factors biasing each record, we consider 'best' estimates referenced in the literature for the size of the CIE in atmospheric CO_2 and marine DIC. Using a benthic foraminiferal record from a paleodepth of ∼1500 m, McCarren et al. (2008) argued for a marine DIC CIE of −3.5‰, while an *n*-alkane record from the same site showed a CIE of −5‰. If these values are representative of the marine and atmospheric CIE sizes, then the ratio of 0.7 suggests an onset duration between 367 and 1989 yr for $\delta^{13}C$ input between −12‰ and −60‰ (1392–1989 yr for a −22‰ to −60‰ source).

Our experiments might hence suggest that available datasets for the PETM constrain the duration of carbon release at the onset of the PETM to less than 2000 yr. In general, amplification of the apparent atmospheric $\delta^{13}C$ excursion relative to mean ocean DIC suggests an onset more rapid than 10 kyr. This contrasts with previous work suggesting that it was not possible to constrain the period of carbon release anywhere between "geologically instantaneous" and 50 kyr (Sluijs et al., 2012). However, this interpretation rests on the assumption that larger terrestrial $\delta^{13}C$ excursions are representative of the atmospheric CO_2 isotopic history and that the −3.5‰ benthic foraminiferal CIE recorded at Walvis Ridge ODP Site 1263 in the South Atlantic is representative of mean global DIC (McCarren et al., 2008).

If either −5‰ overestimates the size of the PETM atmospheric CIE or −3.5‰ underestimates the size of the PETM CIE in DIC, then 2000 yr may be an underestimate of the carbon input duration. Originally, larger terrestrial CIEs were considered the result of changes in soil moisture and humidity, though Pagani et al. (2006) argued that such processes could not explain the −5‰ CIE preserved in *n*-alkanes from the Arctic. Attempts to account for changes in plant fractionation as a function of climate have resulted in an estimate of −4.6‰ for the atmospheric CO_2 CIE

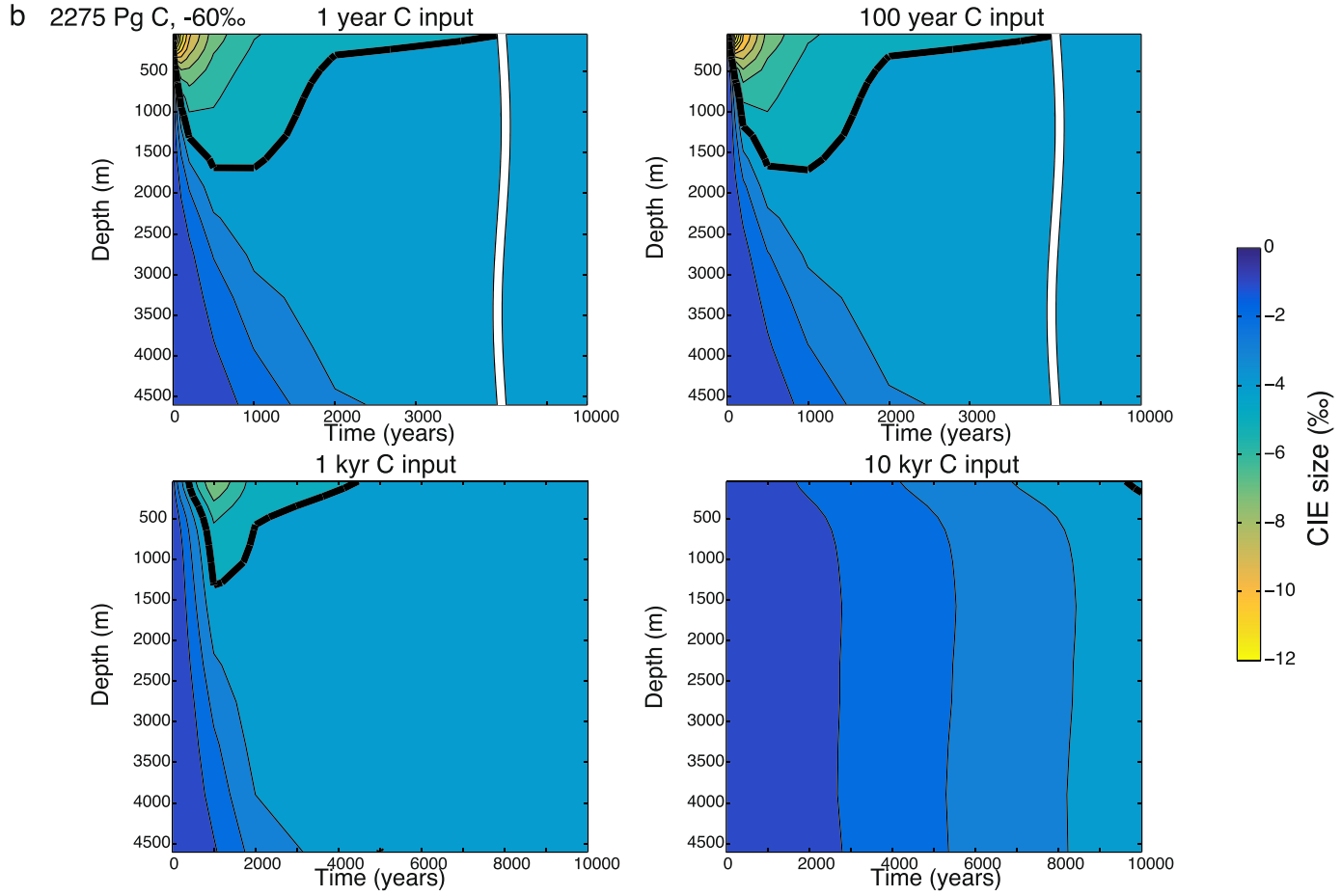

Fig. 6. (*continued*)

based on an *n*-alkane excursion of −5‰ recorded in the Bighorn Basin of North America (Diefendorf et al., 2010; Smith et al., 2007). However, recent work has suggested that plant ^{13}C fractionation was relatively insensitive to changing pCO_2 across the late Paleocene to early Eocene, though the study resolved climate changes over much longer timescales compared to the PETM (Diefendorf et al., 2015). Assuming a −4.6‰ atmospheric CIE and a −3.5‰ marine CIE, our empirical relationship suggests an onset duration <2551 yr (see Eq. (1) and Table S3).

Regarding the possibility that the benthic foraminiferal −3.5‰ CIE from Walvis Ridge is an underestimate of the mean global DIC CIE size – while larger benthic foraminiferal CIEs have been recorded, these come from shallow locations of ∼100 m water depth (e.g., Zachos et al., 2006). Such records are more likely to represent the surface DIC pool and hence be amplified relative to the global DIC CIE. Marine carbonate $\delta^{13}C$ records are often biased towards recording smaller size excursions because of dissolution of deep sea carbonates and bioturbational mixing (Kirtland Turner and Ridgwell, 2013), together with the common practice of averaging multiple foraminiferal specimens in a stratigraphic interval to obtain sufficient mass for an isotopic measurement. The latter issue is sometimes overcome by measuring individual foraminifera, but this practice is rarely successful across the onset of the PETM, where benthic foraminiferal abundances decline and individual specimens are often too small to measure (McCarren et al., 2008; Thomas et al., 2002; Thomas, 2003). Yet even measurements from deep-sea single benthic foraminifera do not show CIEs exceeding −3.5‰ (Thomas et al., 2002; Zachos et al., 2007). We thus consider a −3.5‰ CIE a reasonable (albeit minimum) estimate for the mean global DIC CIE.

Conversely, is it possible that available data lead us to overestimate the duration of carbon release? As Fig. 3 indicates, the amplified CIE in atmospheric CO_2 and surface ocean DIC persists only for a short interval relative to the total event duration. Thus, it may only be possible to detect such amplification if the resolution of a record is greater than a few thousand years; it is possible that low sedimentation rates mean the true amplitude of the atmospheric CO_2 or surface ocean DIC excursion has not been preserved in any analyzed sections. Promisingly, sites with exceptionally high sedimentation rates across the PETM, like those from shallow water sites on the continental margin of the eastern United States, do show larger CIEs in bulk carbonate, planktonic foraminifera and benthic foraminifera compared to deep-sea records, consistent with the idea that these records sample the surface (or near-surface) DIC pool with high fidelity (Wright and Schaller, 2013; Zachos et al., 2006). Well-preserved planktonic foraminiferal records from mixed-layer dwellers also show relatively larger CIEs compared to deep sea benthic foraminiferal $\delta^{13}C$ records, consistent with the idea of surface ocean DIC $\delta^{13}C$ amplification (Zachos et al., 2007). Thus, at least some amplification of atmosphere and surface ocean CIEs is apparent, arguing against an onset much longer than 3000 yr.

Severe ocean acidification (or the development of undersaturated surface ocean conditions) could preclude measurements of amplified surface ocean $\delta^{13}C$ excursions, though out of all of our experiments, only a 1-year emission of the full 14 578 Pg C (−12‰) drives the mean surface ocean undersaturated (Fig. S6). For a 2000-year release of 6856 Pg C (−22‰), no locations in the surface ocean become undersaturated (Fig. S7).

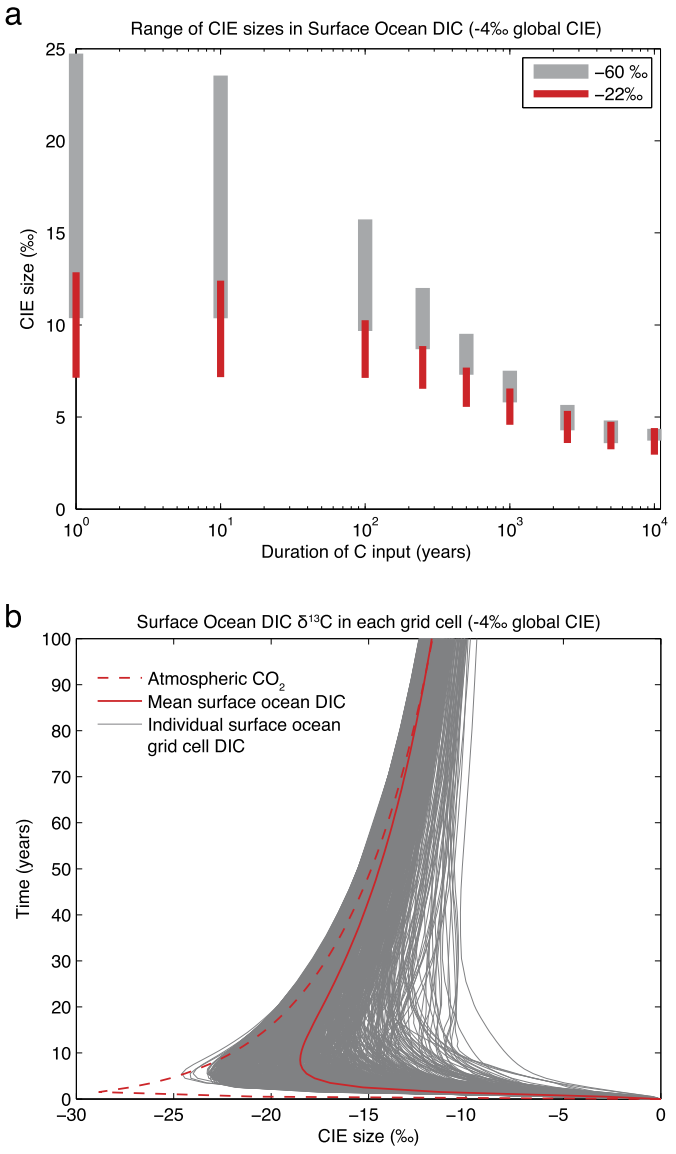

Fig. 7. a) Range in surface ocean DIC CIE sizes as a function of the duration of carbon input for −22‰ carbon input of 6856 Pg C (red bars) and −60‰ carbon input of 2275 Pg C (grey bars). Duration of carbon release is plotted on a log scale. b) Time series of δ^{13}C in surface ocean DIC for every wet grid cell following a 1 yr input of 2275 Pg C of −60‰ (grey lines). Solid red line indicates the mean times series of δ^{13}C in surface ocean DIC and dashed red line indicates the time series of δ^{13}C in atmospheric CO_2. All δ^{13}C time series are adjusted relative to zero to show the size of the CIE rather than absolute δ^{13}C values. (For interpretation of the references to color in this figure legend, the reader is referred to the web version of this article.)

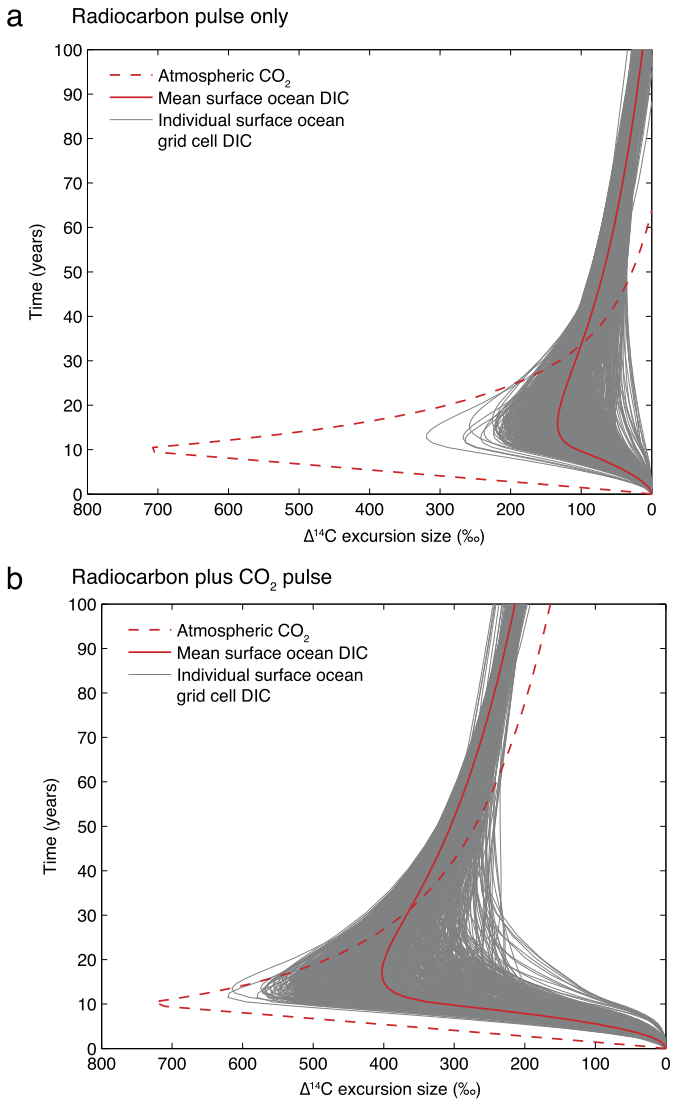

Fig. 8. a) Time series of Δ^{14}C in DIC for every wet grid cell in the surface ocean when atmospheric CO_2 Δ^{14}C is forced to follow a positive excursion of 764.6‰ in 10 yr (grey lines). Solid red line indicates the mean times series of Δ^{14}C in surface ocean DIC and dashed red line indicates the time series of Δ^{14}C in atmospheric CO_2. All Δ^{14}C time series are adjusted relative to zero to show the size of the Δ^{14}C excursion rather than absolute Δ^{14}C values. b) Time series of Δ^{14}C in DIC for every wet grid cell in the surface ocean when atmospheric CO_2 Δ^{14}C is forced to follow a positive excursion of 764.6‰ in 10 yr accompanied by the release of 2275 Pg C to the atmosphere. Solid red line indicates the mean times series of Δ^{14}C in surface ocean DIC and dashed red line indicates the time series of Δ^{14}C in atmospheric CO_2. All Δ^{14}C time series are adjusted relative to zero to show the size of the Δ^{14}C excursion rather than absolute Δ^{14}C values. (For interpretation of the references to color in this figure legend, the reader is referred to the web version of this article.)

3.5. *Propagating a CIE through the exogenic carbon system*

One line of evidence supporting a rapid CO_2 injection into the atmosphere at the PETM onset is the observation of single mixed layer planktonic foraminiferal measurements that show no intermediate values at the PETM onset and a delay of 6–14 kyr between the appearance of excursion values in mixed-layer planktonic foraminifera and in benthic foraminifera at ODP Site 690 in the Southern Ocean (Bralower et al., 2014; Thomas et al., 2002; Zachos et al., 2007, 2003). There is also a substantial delay (stratigraphically, 8 cm) between the δ^{13}C minimum in mixed layer and thermocline planktonic foraminifera (Thomas et al., 2002). However, this ∼5–10 kyr lag (Bralower et al., 2014) is long relative to the mixing time of the global ocean (ca. 1000 yr), suggesting some combination of preservation artefacts (i.e. sedimentary reworking) and/or a significant slowing of vertical mixing rates (Zachos et al., 2007).

Our experiments demonstrate that the propagation time of a CIE with ocean depth is exponentially related to the carbon input duration (Figs. 5 and 6). For larger masses of carbon and short input durations, the delay to propagate the δ^{13}C minimum to the deep ocean increases to >4000 yr. However, these results are global averages, disguising heterogeneity in the vertical propagation time of the δ^{13}C minimum. Individual locations – such as near sites influenced by relatively old waters – could see even longer delays in propagating the δ^{13}C minimum. Thus, the inferred large temporal delay between the appearance of excursion δ^{13}C values in mixed-layer planktonic foraminifera versus benthic species is plausible and consistent with very short carbon input durations. In

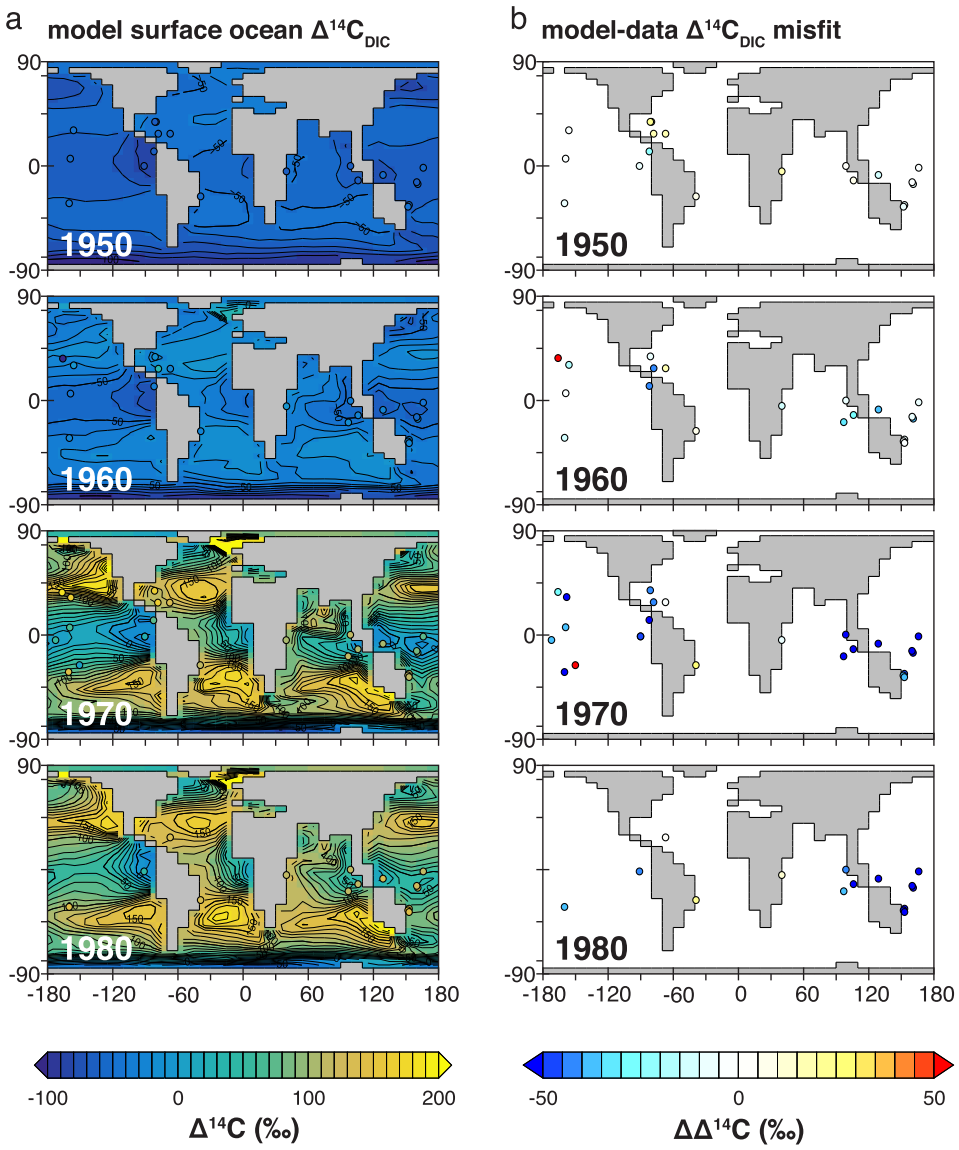

Fig. 9. Evaluation of the $\Delta^{14}C$ perturbation in cGENIE showing a) model surface ocean DIC $\Delta^{14}C$ values in years 1950, 1960, 1970, and 1980 from experiment where CO_2 $\Delta^{14}C$ was forced to follow an excursion of 764.6‰ over 10 yr, and b) the model-data $\Delta^{14}C$ misfit using datasets listed in Table S5.

contrast, the propagation of the $\delta^{13}C$ minimum with depth (Fig. 6) indicates that it cannot take longer than ∼1000 yr for the full mean ocean CIE to reach depths of 1000 m or more (including the impacts of surface warming and transient stratification). This implies that sedimentary reworking (or similar) is required to explain the inferred surface to thermocline delay at ODP Site 690.

3.6. Could the PETM onset be (near) instantaneous?

The purpose of our experiments is to provide a context for interpreting $\delta^{13}C$ records from various reservoirs as they become available. Wright and Schaller (2013) interpreted a −3.5‰ CIE in bulk carbonate from a shallow marine section (<100 m water depth) at Millville (ODP 174X) as evidence for a roughly instantaneous PETM (13 yr onset duration). Based on the necessity to account for the full −3.5‰ CIE in deep ocean DIC and a presumed relationship in the size of bulk carbonate CIEs with depth along the continental margin, they argued that their record was consistent with an atmospheric CO_2 CIE of ∼−20‰ (Wright and Schaller, 2013). They further argued that the −3.5‰ CIE was consistent with an excursion of −20‰ in atmospheric CO_2 by citing the spatially heterogeneous surface ocean records of the bomb radiocarbon perturbation of the last century (Wright and Schaller, 2013). Irrespective of this interpretation of the Millville record, the question of whether the bomb-derived propagation of a $\Delta^{14}C$ transient from the atmosphere into the ocean can shed light on geological $\delta^{13}C$ excursions demands quantitative assessment.

To test the applicability of the bomb radiocarbon anomaly as an analogy for rapid release of ^{13}C-depleted carbon at the PETM, we ran a series of experiments to approximate the historical bomb radiocarbon perturbation. For these experiments, the configuration of the cGENIE model used was that of Cao et al. (2009), which has the same resolution as the configuration used for the Eocene experiments described above, but does not include sediments or weathering. Experiments were run following a 10 000 yr spin-up to equilibrate ocean circulation and climate, with atmospheric pCO_2 set at a pre-industrial concentration of 278 ppm with a $\delta^{13}C$ of −6.5‰ and $\delta^{14}C$ of 38.4‰ (i.e. atmospheric $\Delta^{14}C = \sim 0$‰). In the first experiment, atmospheric pCO_2 was held constant at 278 ppm while CO_2 $\Delta^{14}C$ was forced to follow an excursion of 764.6‰ in 10 yr. In the second, CO_2 $\Delta^{14}C$ was forced to follow the same excursion, but at the same time, the atmospheric CO_2 inventory

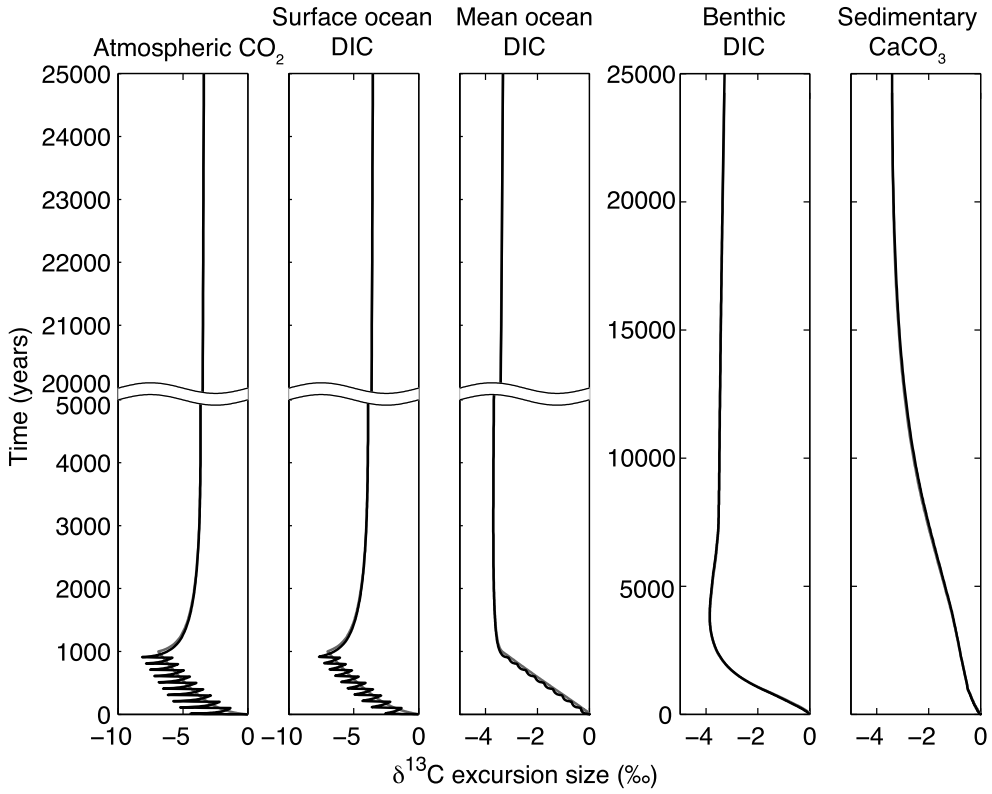

Fig. 10. Comparison of the time history of $\delta^{13}C$ in each carbon reservoir for a 2275 Pg C of −60‰ over 1000 yr at a constant rate of 2.275 Pg C yr^{-1} (grey lines) versus a pulsed release of carbon at 22.75 Pg C yr^{-1} for 10 yr, followed by 90 yr of no carbon release repeated for 1000 yr (black lines). Results are shown (from left to right) for atmospheric CO_2, surface ocean DIC, mean ocean DIC, benthic DIC, and sedimentary $CaCO_3$.

was increased by 2275 Pg C (for comparison with a PETM carbon release scenario). Each experiment was then run for a total of 1000 yr without additional forcing.

When atmospheric CO_2 $\Delta^{14}C$ is forced to follow an approximate ∼700‰ historical positive over 10 yr, the average surface ocean DIC $\Delta^{14}C$ excursion is just over 100‰, with a minimum of almost 0‰ and a maximum of ∼300‰ (Fig. 8a). This reduction in excursion magnitude is consistent with records from corals of the surface ocean DIC $\Delta^{14}C$ excursion that show magnitudes up to 9× smaller than the known atmospheric $\Delta^{14}C$ history (Rodgers et al., 2000), shown in Fig. 9 (see also Table S5). In contrast, in our second experiment, where atmospheric CO_2 $\Delta^{14}C$ follows the same trajectory, but is accompanied by a release of 2275 Pg C, the resulting distribution of surface ocean DIC $\Delta^{14}C$ excursions much more closely resembles our results from the Eocene ^{13}C-depelted carbon release scenario (Fig. 8b compared to Fig. 7b). In this case, the average surface ocean DIC $\Delta^{14}C$ excursion is ∼400‰, with a minimum of ∼250‰ and a maximum of ∼600‰. In other words, the minimum surface ocean DIC $\Delta^{14}C$ excursion is just over 1/3 of the size of the atmospheric CO_2 $\Delta^{14}C$ excursion. Our Eocene experiments further demonstrated that the range of CIEs in the surface ocean would be relatively smaller for a rapid release of larger masses of CO_2 (Fig. 7a), suggesting that 1/3 of the size of the atmospheric excursion is a minimum for surface ocean records.

Our experiments thus suggest that the $\Delta^{14}C$ perturbation of the past century is a poor analogy for the range in surface ocean DIC CIEs possible from an instantaneous release of ^{13}C-depleted carbon (Fig. 8). This is because the dynamics of an isotopic perturbation alone are very different from an isotopic perturbation accompanied by a large release of CO_2. What happens is that the increase in air–sea gas exchange caused by the bulk carbon release drives the average surface DIC isotopic composition closer to the atmospheric isotopic composition because carbon and its isotopes are more rapidly exchanged with the surface ocean.

Zeebe et al. (2014) also argued that the CIE measured by Wright and Schaller (2013) was too small to reflect carbon release over a decade by comparing a modeled mean surface ocean DIC isotopic history to the atmosphere isotopic history following an instant pulse of carbon. Our analysis goes a step further to quantify the likely range in surface ocean CIE sizes. Applying either of the preferred release scenarios of 2275 Pg C of −60‰ or 6856 Pg C of −22‰ over 10 yr yields an atmospheric CO_2 CIE of ∼−12‰ or −24‰, with a minimum surface ocean CIE of ∼7.5‰ or 11‰ (see Fig. 7a). While mixing may truncate the sedimentary expression of an excursion originally recorded in the surface ocean by nannofossils or planktonic foraminifera, a sedimentary sequence with a very high accumulation rate (especially the proposed annual resolution, Wright and Schaller, 2013) should not be notably biased (Kirtland Turner and Ridgwell, 2013).

3.7. Reconciling conflicting estimates of onset duration

Our cGENIE experiments consider the release of carbon at a constant rate equal to the mass of carbon divided by the total release duration in years. These experiments thus disguise the (likely) possibility that carbon release did not occur at a constant rate. As a final example, we consider the difference between emitting 2275 Pg C of −60‰ over 1000 yr at a constant rate of 2.275 Pg C yr^{-1} compared to a scenario where carbon was released at 22.75 Pg C yr^{-1} for 10 yr, followed by 90 yr of no carbon release, before resuming carbon release at 22.75 Pg C yr^{-1} at the start of the following century (Fig. 10). This latter scenario still equates to an average emission rate of 2.275 Pg C yr^{-1} for 1000 yr, though these two scenarios could result in very different records in sites

with very high sedimentary accumulation rates or that only record part of the event.

If carbon was released in extremely short pulses, each individual pulse would generate an excursion in atmospheric CO_2 and surface ocean DIC. In our example scenario, there are thus 10 separate $\sim -3‰$ CIEs pasted on top of an overall 1000 yr excursion. However, the mean ocean DIC, benthic DIC and sedimentary $CaCO_3$ records of this emissions scenario are identical to the release of carbon at an average rate of just 2.275 Pg C yr^{-1} for 1000 yr (Fig. 10). In this way, it would be possible for a sedimentary section with extremely high accumulation rates to record just one of a series of CIEs and thus show a relatively small size compared to what would be required were the entire mass of carbon to have been released at once.

Is a scenario consisting of multiple phases of emissions likely? This style of emissions is potentially consistent with the idea that the PETM was caused by a series of carbon cycle feedbacks (DeConto et al., 2012; Zachos et al., 2010) following a long-term warming trend. It is also consistent with repeated injections of carbon as a result of volcanic intrusion into organic rich material, e.g. Svensen et al. (2004).

4. Conclusions

We used an Earth system model to evaluate the effect of the duration of release of a ^{13}C-depleted pulse of carbon on the magnitude and time history of the CIE recorded in various reservoirs of the exogenic carbon system. While these experiments were designed to test various emissions scenarios consistent with available constraints for the PETM, the results are generally applicable to other purported episodes of major carbon release in Earth history. We have generated an empirical relationship between the ratio of the CIE in mean ocean DIC to atmospheric CO_2 and the duration of carbon input. When applied using available PETM records, we inferred the duration of onset to have been <3000 yr, though we emphasize that constraints on additional sources of error in interpreting atmosphere and ocean $\delta^{13}C$ excursion magnitudes are crucial. This empirical relationship provides a framework for interpreting new PETM records as they become available and suggests that the amplification of terrestrial and surface ocean CIEs is consistent with a rapid rate of carbon release and need not be fully explained by factors that artificially enhance the apparent CIE in terrestrial proxies or dampen the CIE in marine proxies. However, such biases are possible and must be considered before this metric can be confidently applied to any particular geologic carbon release episode. In particular, better mechanistic understanding of the factors controlling $\delta^{13}C$ signals in organic matter and those that influence the sedimentary preservation of $\delta^{13}C$ signals in the deep sea is crucial. Still, the significant difference between available marine and terrestrial records might, in and of itself, provide a useful metric for constraining the rate of carbon release across the PETM, and potentially across similar events in Earth history as well.

Acknowledgements

This work was funded by an NSF International Research Fellowship to SKT (1159100). A Ridgwell acknowledges support via EU grant ERC-2013-CoG-617313. The authors also thank Lee Kump for helpful suggestions that improved the final text.

Appendix A. Supplementary material

Supplementary material related to this article can be found online at http://dx.doi.org/10.1016/j.epsl.2015.11.027.

References

Bowen, G.J., Beitler Bowen, B., 2008. Mechanisms of PETM global change constrained by a new record from central Utah. Geology 36 (5), 379–382.
Bralower, T.J., Meissner, K.J., Alexander, K., Thomas, D.J., 2014. The dynamics of global change at the Paleocene–Eocene thermal maximum: a data-model comparison. Geochem. Geophys. Geosyst. 15 (10), 3830–3848.
Cao, L., Eby, M., Ridgwell, A., Caldeira, K., Archer, D., Ishida, A., Joos, F., Matsumoto, K., Mikolajewicz, U., Mouchet, A., Orr, J.C., Plattner, G.K., Schlitzer, R., Tokos, K., Totterdell, I., Tschumi, T., Yamanaka, Y., Yool, A., 2009. The role of ocean transport in the uptake of anthropogenic CO_2. Biogeosciences 6 (3), 375–390.
Colbourn, G., Ridgwell, A., Lenton, T., 2013. The rock geochemical model (RokGeM) v0. 9. Geosci. Model Dev. 6 (5), 1543–1573.
Cui, Y., Kump, L.R., Ridgwell, A.J., Charles, A.J., Junium, C.K., Diefendorf, A.F., Freeman, K.H., Urban, N.M., Harding, I.C., 2011. Slow release of fossil carbon during the Palaeocene–Eocene thermal maximum. Nat. Geosci. 4 (7), 481–485.
DeConto, R.M., Galeotti, S., Pagani, M., Tracy, D., Schaefer, K., Zhang, T., Pollard, D., Beerling, D.J., 2012. Past extreme warming events linked to massive carbon release from thawing permafrost. Nature 484 (7392), 87–91.
Diefendorf, A.F., Mueller, K.E., Wing, S.L., Koch, P.L., Freeman, K.H., 2010. Global patterns in leaf ^{13}C discrimination and implications for studies of past and future climate. Proc. Natl. Acad. Sci. 107 (13), 5738–5743.
Diefendorf, A.F., Freeman, K.H., Wing, S.L., Currano, E.D., Mueller, K.E., 2015. Paleogene plants fractionated carbon isotopes similar to modern plants. Earth Planet. Sci. Lett. 429, 33–44.
Dunkley Jones, T., Lunt, D.J., Schmidt, D.N., Ridgwell, A., Sluijs, A., Valdes, P.J., Maslin, M., 2013. Climate model and proxy data constraints on ocean warming across the Paleocene–Eocene thermal maximum. Earth-Sci. Rev. 125 (0), 123–145.
Dunkley Jones, T., Ridgwell, A., Lunt, D.J., Maslin, M.A., Schmidt, D.N., Valdes, P.J., 2010. A Paleogene perspective on climate sensitivity and methane hydrate instability. Philos. Trans. R. Soc. A, Math. Phys. Eng. Sci. 368 (1919), 2395–2415.
Edwards, N., Marsh, R., 2005. Uncertainties due to transport-parameter sensitivity in an efficient 3-D ocean–climate model. Clim. Dyn. 24 (4), 415–433.
Farley, K.A., Eltgroth, S.F., 2003. An alternative age model for the Paleocene–Eocene thermal maximum using extraterrestrial ^{3}He. Earth Planet. Sci. Lett. 208 (3–4), 135–148.
Hönisch, B., Ridgwell, A., Schmidt, D.N., Thomas, E., Gibbs, S.J., Sluijs, A., Zeebe, R., Kump, L., Martindale, R.C., Greene, S.E., Kiessling, W., Ries, J., Zachos, J.C., Royer, D.L., Barker, S., Marchitto, T.M., Moyer, R., Pelejero, C., Ziveri, P., Foster, G.L., Williams, B., 2012. The geological record of ocean acidification. Science 335 (6072), 1058–1063.
Kirtland Turner, S., Ridgwell, A., 2013. Recovering the true size of an Eocene hyperthermal from the marine sedimentary record. Paleoceanography 28 (4), 700–712.
Marchal, O., Stocker, T.F., Joos, F., 1998. A latitude-depth, circulation-biogeochemical ocean model for paleoclimate studies. Development and sensitivities. Tellus B 50 (3), 290–316.
McCarren, H., Thomas, E., Hasegawa, T., Röhl, U., Zachos, J.C., 2008. Depth dependency of the Paleocene–Eocene carbon isotope excursion: paired benthic and terrestrial biomarker records (Ocean Drilling Program Leg 208, Walvis Ridge). Geochem. Geophys. Geosyst. 9 (10), Q10008.
McInerney, F.A., Wing, S.L., 2011. The Paleocene–Eocene thermal maximum: a perturbation of carbon cycle, climate, and biosphere with implications for the future. Annu. Rev. Earth Planet. Sci. 39 (1), 489–516.
Mook, W.G., 1986. ^{13}C in atmospheric CO_2. Neth. J. Sea Res. 20 (2–3), 211–223.
Pagani, M., Pedentchouk, N., Huber, M., Sluijs, A., Schouten, S., Brinkhuis, H., Sinninghe Damste, J.S., Dickens, G.R., Expedition, S., 2006. Arctic hydrology during global warming at the Palaeocene/Eocene thermal maximum. Nature 442 (7103), 671–675.
Panchuk, K., 2007. Investigating the Paleocene/Eocene carbon cycle perturbation: an Earth system model approach. PhD thesis. Pennsylvania State University, State College, Pennsylvania, USA.
Panchuk, K., Ridgwell, A., Kump, L.R., 2008. Sedimentary response to Paleocene–Eocene thermal maximum carbon release: a model-data comparison. Geology 36 (4), 315–318.
Peters, G.P., Marland, G., Le Quere, C., Boden, T., Canadell, J.G., Raupach, M.R., 2012. Rapid growth in CO_2 emissions after the 2008–2009 global financial crisis. Nat. Clim. Change 2 (1), 2–4.
Rau, G., Riebesell, U., Wolf-Gladrow, D., 1996. A model of photosynthetic ^{13}C fractionation by marine phytoplankton based on diffusive molecular CO_2 uptake. Mar. Ecol. Prog. Ser. 133, 275–285.
Ridgwell, A., 2001. Glacial–interglacial perturbations in the global carbon cycle. PhD thesis. University of East Anglia at Norwich, Norwich, UK.
Ridgwell, A., 2007. Interpreting transient carbonate compensation depth changes by marine sediment core modeling. Paleoceanography 22 (4), PA4102.
Ridgwell, A., Hargreaves, J., 2007. Regulation of atmospheric CO_2 by deep-sea sediments in an Earth system model. Glob. Biogeochem. Cycles 21 (2).
Ridgwell, A., Hargreaves, J., Edwards, N.R., Annan, J., Lenton, T.M., Marsh, R., Yool, A., Watson, A., 2007. Marine geochemical data assimilation in an efficient Earth System Model of global biogeochemical cycling. Biogeosciences 4 (1), 87–104.

Ridgwell, A., Schmidt, D.N., 2010. Past constraints on the vulnerability of marine calcifiers to massive carbon dioxide release. Nat. Geosci. 3 (3), 196–200.
Rodgers, K.B., Schrag, D.P., Cane, M.A., Naik, N.H., 2000. The bomb ^{14}C transient in the Pacific Ocean. J. Geophys. Res., Oceans 105 (C4), 8489–8512.
Rohl, U., Westerhold, T., Bralower, T.J., Zachos, J.C., 2007. On the duration of the Paleocene–Eocene thermal maximum (PETM). Geochem. Geophys. Geosyst. 8, Q12002.
Schmittner, A., Gruber, N., Mix, A., Key, R., Tagliabue, A., Westberry, T., 2013. Biology and air–sea gas exchange controls on the distribution of carbon isotope ratios ($\delta^{13}C$) in the ocean. Biogeosciences 10 (9), 5793–5816.
Schouten, S., Woltering, M., Rijpstra, W.I.C., Sluijs, A., Brinkhuis, H., Sinninghe Damsté, J.S., 2007. The Paleocene–Eocene carbon isotope excursion in higher plant organic matter: differential fractionation of angiosperms and conifers in the Arctic. Earth Planet. Sci. Lett. 258 (3–4), 581–592.
Sluijs, A., Dickens, G.R., 2012. Assessing offsets between the $\delta^{13}C$ of sedimentary components and the global exogenic carbon pool across early Paleogene carbon cycle perturbations. Glob. Biogeochem. Cycles 26 (4), GB4005.
Sluijs, A., Zachos, J.C., Zeebe, R.E., 2012. Constraints on hyperthermals. Nat. Geosci. 5 (4), 231.
Smith, F.A., Wing, S.L., Freeman, K.H., 2007. Magnitude of the carbon isotope excursion at the Paleocene–Eocene thermal maximum: the role of plant community change. Earth Planet. Sci. Lett. 262 (1–2), 50–65.
Svensen, H., Planke, S., Malthe-Sorenssen, A., Jamtveit, B., Myklebust, R., Rasmussen Eidem, T., Rey, S.S., 2004. Release of methane from a volcanic basin as a mechanism for initial Eocene global warming. Nature 429 (6991), 542–545.
Thomas, D.J., Zachos, J.C., Bralower, T.J., Thomas, E., Bohaty, S., 2002. Warming the fuel for the fire: evidence for the thermal dissociation of methane hydrate during the Paleocene–Eocene thermal maximum. Geology 30 (12), 1067–1070.
Thomas, E., 2003. Extinction and food at the seafloor: a high-resolution benthic foraminiferal record across the initial Eocene thermal maximum. In: Southern Ocean Site 690 in Causes and Consequences of Globally Warm Climates in the Early Paleogene. Spec. Pap., Geol. Soc. Am. 369, 319–332.
Wanninkhof, R., 1992. Relationship between wind speed and gas exchange over the ocean. J. Geophys. Res., Oceans 97 (C5), 7373–7382.
Wright, J.D., Schaller, M.F., 2013. Evidence for a rapid release of carbon at the Paleocene–Eocene thermal maximum. Proc. Natl. Acad. Sci. 110 (40), 15908–15913.
Zachos, J.C., Bohaty, S.M., John, C.M., McCarren, H., Kelly, D.C., Nielsen, T., 2007. The Palaeocene–Eocene carbon isotope excursion: constraints from individual shell planktonic foraminifer records. Philos. Trans. R. Soc. A, Math. Phys. Eng. Sci. 365 (1856), 1829–1842.
Zachos, J.C., Dickens, G.R., Zeebe, R.E., 2008. An early Cenozoic perspective on greenhouse warming and carbon-cycle dynamics. Nature 451, 279–283.
Zachos, J.C., McCarren, H., Murphy, B., Rohl, U., Westerhold, T., 2010. Tempo and scale of late Paleocene and early Eocene carbon isotope cycles: implications for the origin of hyperthermals. Earth Planet. Sci. Lett. 299 (1–2), 242–249.
Zachos, J.C., Rohl, U., Schellenberg, S.A., Sluijs, A., Hodell, D.A., Kelly, D.C., Thomas, E., Nicolo, M., Raffi, I., Lourens, L.J., McCarren, H., Kroon, D., 2005. Rapid acidification of the ocean during the Paleocene–Eocene thermal maximum. Science 308 (5728), 1611–1615.
Zachos, J.C., Schouten, S., Bohaty, S., Quattlebaum, T., Sluijs, A., Brinkhuis, H., Gibbs, S.J., Bralower, T.J., 2006. Extreme warming of mid-latitude coastal ocean during the Paleocene–Eocene thermal maximum: inferences from TEX86 and isotope data. Geology 34 (9), 737–740.
Zachos, J.C., Wara, M.W., Bohaty, S., Delaney, M.L., Petrizzo, M.R., Brill, A., Bralower, T.J., Premoli-Silva, I., 2003. A transient rise in tropical sea surface temperature during the Paleocene–Eocene thermal maximum. Science 302 (5650), 1551–1554.
Zeebe, R.E., Dickens, G.R., Ridgwell, A., Sluijs, A., Thomas, E., 2014. Onset of carbon isotope excursion at the Paleocene–Eocene thermal maximum took millennia, not 13 years. Proc. Natl. Acad. Sci. 111 (12), E1062–E1063.
Zeebe, R.E., Wolf-Gladrow, D.A., 2001. CO_2 in Seawater: Equilibrium, Kinetics, Isotopes. Gulf Professional Publishing.
Zeebe, R.E., Zachos, J.C., Dickens, G.R., 2009. Carbon dioxide forcing alone insufficient to explain Palaeocene–Eocene thermal maximum warming. Nat. Geosci. 2 (8), 576–580.
Zhang, J., Quay, P.D., Wilbur, D.O., 1995. Carbon isotope fractionation during gas–water exchange and dissolution of CO_2. Geochim. Cosmochim. Acta 59 (1), 107–114.